

# Catalytic Function of the PR-Set7 Histone H4 Lysine 20 Monomethyltransferase Is Essential for Mitotic Entry and Genomic Stability<sup>\*[5]</sup>

Received for publication, December 31, 2007, and in revised form, March 31, 2008. Published, JBC Papers in Press, May 14, 2008, DOI 10.1074/jbc.M710579200

Sabrina I. Houston<sup>†1</sup>, Kirk J. McManus<sup>§</sup>, Melissa M. Adams<sup>¶</sup>, Jennifer K. Sims<sup>‡</sup>, Phillip B. Carpenter<sup>¶1,2</sup>, Michael J. Hendzel<sup>§</sup>, and Judd C. Rice<sup>‡3</sup>

From the <sup>†</sup>Department of Biochemistry and Molecular Biology, University of Southern California Keck School of Medicine, Los Angeles, California 90033, the <sup>§</sup>Department of Oncology, University of Alberta, Cross Cancer Institute, Edmonton, Alberta T6G 1Z2, Canada, and the <sup>¶</sup>Department of Biochemistry and Molecular Biology, University of Texas Health Science Center, Houston, Texas 77030

Histone-modifying enzymes play a critical role in modulating chromatin dynamics. In this report we demonstrate that one of these enzymes, PR-Set7, and its corresponding histone modification, the monomethylation of histone H4 lysine 20 (H4K20), display a distinct cell cycle profile in mammalian cells: low at G<sub>1</sub>, increased during late S phase and G<sub>2</sub>, and maximal from prometaphase to anaphase. The lack of PR-Set7 and monomethylated H4K20 resulted in a number of aberrant phenotypes in several different mammalian cell types. These include the inability of cells to progress past G<sub>2</sub>, global chromosome condensation failure, aberrant centrosome amplification, and substantial DNA damage. By employing a catalytically dead dominant negative PR-Set7 mutant, we discovered that its mono-methyltransferase activity was required to prevent these phenotypes. Importantly, we demonstrate that all of the aberrant phenotypes associated with the loss of PR-Set7 enzymatic function occur independently of p53. Collectively, our findings demonstrate that PR-Set7 enzymatic activity is essential for mammalian cell cycle progression and for the maintenance of genomic stability, most likely by monomethylating histone H4K20. Our results predict that alterations of this pathway could result in gross chromosomal aberrations and aneuploidy.

Dynamic alterations in chromatin structure are modulated, in part, by the post-translational modifications of the DNA-associated histone proteins. Specialized chromatin-modifying enzymes can phosphorylate, acetylate, ubiquitylate, or methyl-

ate specific amino acids within certain histones, and each of these modifications are associated with distinct biological events (1). One of the first histone modifications to be identified nearly forty-five years ago was the methylation of histone H4 lysine 20 (H4K20)<sup>4</sup> (2). Earlier biochemical studies linked H4K20 methylation to diverse biological events including transcriptional regulation, chromatin compaction, cell division, and the formation of heterochromatin (3–9). Importantly, it was also found that H4K20 is differentially methylated *in vivo* and therefore can be either mono-, di-, or trimethylated (10). Together, these findings strongly suggest that different methylated states of H4K20 may be involved in distinct biological processes, similar to what is observed for the various methylated states of histone H3 lysine 4 and 9 methylation (11, 12).

Increasing evidence indicates that certain enzymes are responsible for the specific degree of histone lysine methylation (13). For example, the mono- and dimethylation of histone H3 lysine 9 in humans is mediated by the G9a enzyme, whereas trimethylation is mediated by the SUV39H1 enzyme (14, 15). Similarly, the Suv4–20 enzymes are responsible for di- and trimethylation in mammals (16, 17). Trimethylated H4K20 is associated with repressed chromatin because it is targeted to constitutive heterochromatin, various repetitive elements, and imprinting control regions (16, 18, 19). Dimethylated H4K40 is more widely distributed within euchromatic regions in the genome, and recent findings suggest that it may function to recruit the 53BP1 repair protein to sites of DNA damage (17, 20, 21).

The PR-Set7 enzyme is responsible for the bulk of H4K20 monomethylation (22–25). Although original observations suggested that this modification was associated with repressed regions of the genome, recent findings have identified monomethylated H4K20 within actively transcribed genes (26, 27). Besides functioning in transcription, it was recently found that PR-Set7 plays a role in mammalian cell cycle progression by binding proliferating cell nuclear antigen and localizing to rep-

<sup>\*</sup> This work was supported, in whole or in part, by National Institutes of Health Grant GM075094 (to J. C. R.). This work was also supported by generous funding from the Donald E. and Delia B. Baxter Foundation and the Robert E. and May R. Wright Foundation. The costs of publication of this article were defrayed in part by the payment of page charges. This article must therefore be hereby marked "advertisement" in accordance with 18 U.S.C. Section 1734 solely to indicate this fact.

[5] The on-line version of this article (available at <http://www.jbc.org>) contains supplemental Figs. S1–S5.

<sup>1</sup> Supported by a grant from the California Breast Cancer Research Program.

<sup>2</sup> Supported by the National Institutes of Health Grant R56 GM065812 and by a generous grant from the Robert Welch Foundation Grant AU-1569.

<sup>3</sup> Pew Scholar in the Biomedical Sciences. To whom correspondence should be addressed: Dept. of Biochemistry and Molecular Biology, University of Southern California Keck School of Medicine, 1450 Biggy St., NRT 6506, Los Angeles, CA 90033. Tel.: 323-442-4332; Fax: 323-442-4433; E-mail: juddrice@usc.edu.

<sup>4</sup> The abbreviations used are: H4K20, histone H4 lysine 20; RNAi, RNA interference; WT, wild type; ChIP, chromatin immunoprecipitation; shRNA, small hairpin RNA; GFP, green fluorescent protein; GST, glutathione S-transferase; DAPI, 4',6'-diamino-2-phenylindole; H3S28, histone H3 serine 28; MNase, micrococcal nuclease; TT, tandem tudor domains; CD, catalytically dead.

lication foci (28–30). Although the loss of PR-Set7 by RNAi eventually resulted in defective replication fork activity and delayed S phase progression, several cell cycles were required to achieve this phenotype (29, 30). Furthermore, we previously demonstrated that expression of PR-Set7 was tightly cell cycle-regulated where it was undetectable at G<sub>1</sub>/S, slowly increased during late S phase, and peaked during mitosis, concomitant with its catalytic activity (31). Based on these contradictory observations, it currently remains unclear how PR-Set7 and H4K20 methylation function in mammalian cell cycle progression.

To further investigate this, we first employed a panel of H4K20 methyl-specific antibodies to determine that only the monomethylated form of H4K20 displayed a distinct cell cycle profile: low at G<sub>1</sub>, increased during late S, and highest at G<sub>2</sub>/M, identical to PR-Set7 (32). Furthermore, we also defined that the cell cycle-dependent changes in monomethylated H4K20 occurred locally at specific genomic regions. Similar to recent reports, RNAi-mediated depletion of PR-Set7 and H4K20 monomethylation resulted in delayed S phase progression (29, 30). However, we found that the PR-Set7 RNAi cells were capable of completing S phase and, in a p53-independent manner, arrested at prometaphase, when PR-Set7 and monomethylated H4K20 levels peak. Consistent with recent findings indicating that these factors are important for chromatin compaction, the PR-Set7 RNAi cells displayed enlarged nuclei containing decondensed chromosomes (33, 34). In addition, we observed significant increases in DNA damage and aberrant centrosome amplification in cells lacking PR-Set7, two key events associated with oncogenic transformation. Importantly, we discovered that the catalytic activity of PR-Set7 was required to prevent all these phenotypes. Therefore, our findings indicate that the catalytic function of PR-Set7 is essential for mitotic entry and genomic stability, most likely by directly controlling the levels of monomethylated H4K20.

## EXPERIMENTAL PROCEDURES

**Immunofluorescence**—Indirect immunofluorescence of mouse embryonic fibroblasts was performed as previously described (32). Antibody dilutions were used as follows: H4K20 mono- (1:1,000), di- (1:500), and trimethyl (1:1,000) (LP Biologicals);  $\gamma$ H2AX (Millipore; 1:500); and  $\gamma$ -tubulin (Sigma; 1:400). Staining was visualized on the Zeiss Axio Imager Z1 microscope with Apotome using a Z-stack acquisition, three-dimensional reconstruction, and structured illumination. Volumetric measurements were made using algorithms developed for use with Zeiss proprietary AxioVision software. The pictures were analyzed and prepared with Adobe PhotoShop CS2. Quantitative imaging microscopy was performed on murine 10T1/2 cells using a Zeiss Axioplan 2 microscope equipped with a 12-bit Coolsnap HQ cooled CCD camera and a 40 $\times$  fluor lens, as previously described (35).

**Cell Cycle Synchronization**—HeLa cells were first blocked at the G<sub>1</sub>/S border with 2 mM thymidine for 17 h (31). The cells were then released into fresh medium (Dulbecco's modified Eagle's medium (Invitrogen) plus 10% cosmic calf serum (HyClone)) for 7 h prior to the addition of 400  $\mu$ M L-mimosine

for 20 h. The cells were released into fresh medium and collected every 2.5 h for Western analysis or flow cytometry.

**Western Analysis**—Whole cell lysates from 10<sup>5</sup> cells were fractionated by SDS-PAGE, transferred to a polyvinylidene difluoride membrane, and blocked in 5% nonfat milk/Tris-buffered saline prior to incubation with primary antibody in 1% nonfat milk/Tris-buffered saline for 1 h rotating at room temperature. Antibody dilutions were as follows: H4K20 mono- (1:150,000), di- (1:100,000), or trimethyl (1:20,000) (LP Biologicals); H3K9 mono- (1:60,000), di- (1:80,000), or trimethyl (1:10,000) (Millipore); H4 general (Millipore; 1:100,000); phospho-H3S10 (Serotec; 1:20,000); phospho-H3S28 (1:2000);  $\gamma$ H2AX (Millipore; 1:25,000); phospho-ATM (Rockland; 1:1000); and PR-Set7 (1:1000) dilution. Following three washes in Tris-buffered saline + 0.1% Tween 20, the membranes were incubated with an appropriate horseradish peroxidase-conjugated secondary antibody (Jackson ImmunoResearch; 1:5,000) in 1% nonfat milk/Tris-buffered saline for 1 h at room temperature. The membranes were washed three more times prior to the addition of ECL Plus (GE Healthcare). The results were visualized by exposure to film for 1 min.

**Chromatin Immunoprecipitation (ChIP)**—HeLa cells were fixed in 1% formaldehyde for 10 min before quenching with 0.125 M glycine for 5 min. The nuclei were isolated using nuclear isolation buffer (150 mM NaCl, 10 mM HEPES, pH 7.5, 1.5 mM MgCl<sub>2</sub>, 10 mM KCl, 0.5% Nonidet P-40, 0.5 mM dithiothreitol) and resuspended in nuclear lysis buffer (50 mM Tris-Cl, pH 8.1, 10 mM EDTA, 1% SDS) at a concentration of 10<sup>8</sup> nuclei/ml. The nuclei were sonicated to DNA fragments ranging from 200 to 600 bp. For each ChIP, sonicated nuclear material from 5  $\times$  10<sup>6</sup> cells was immunoprecipitated with either rabbit IgG, a histone H3 general antibody (Abcam), or a histone H4K20 monomethyl-specific antibody (Lake Placid Biologicals). Immune complexes were precipitated with protein A-conjugated Sepharose (Amersham Biosciences and GE Biosciences) and washed with radioimmune precipitation assay buffer (50 mM HEPES, pH 7.4, 1 mM EDTA, 1% Nonidet P-40, 0.7% sodium deoxycholate, 500 mM LiCl). DNA was eluted using a 10% Chelex (Bio-Rad) solution (36).

**PR-Set7 shRNA and CD Mutant**—A pSUPERIOR.retro.puro empty vector (OligoEngine) or the vector containing either a nonspecific shRNA sequence (5'-TCGCCTAGGAAGACTGATC-3') or an shRNA targeted to PR-Set7 (5'-ACGCAACA-GAATCGCAAAC-3') were transfected into HCT116 and HEK 293 cells using Lipofectamine 2000 (Invitrogen) according to the manufacturer's protocol. Puromycin selection (4  $\mu$ g/ml for HEK 293, 1  $\mu$ g/ml for HCT116) was initiated 1 day post-transfection. Whole cell lysates were collected 6 days post-transfection for Western analysis. A pQCXIP vectors (Clontech) containing either enhanced GFP or the full-length PR-Set7 R265G dominant negative mutant were transfected into HCT116 and HEK 293 cells using Lipofectamine 2000 (24). The samples were collected 3 days following puromycin selection for Western analysis and flow cytometry. For growth curves, the cells were counted manually beginning 2 days following puromycin selection.

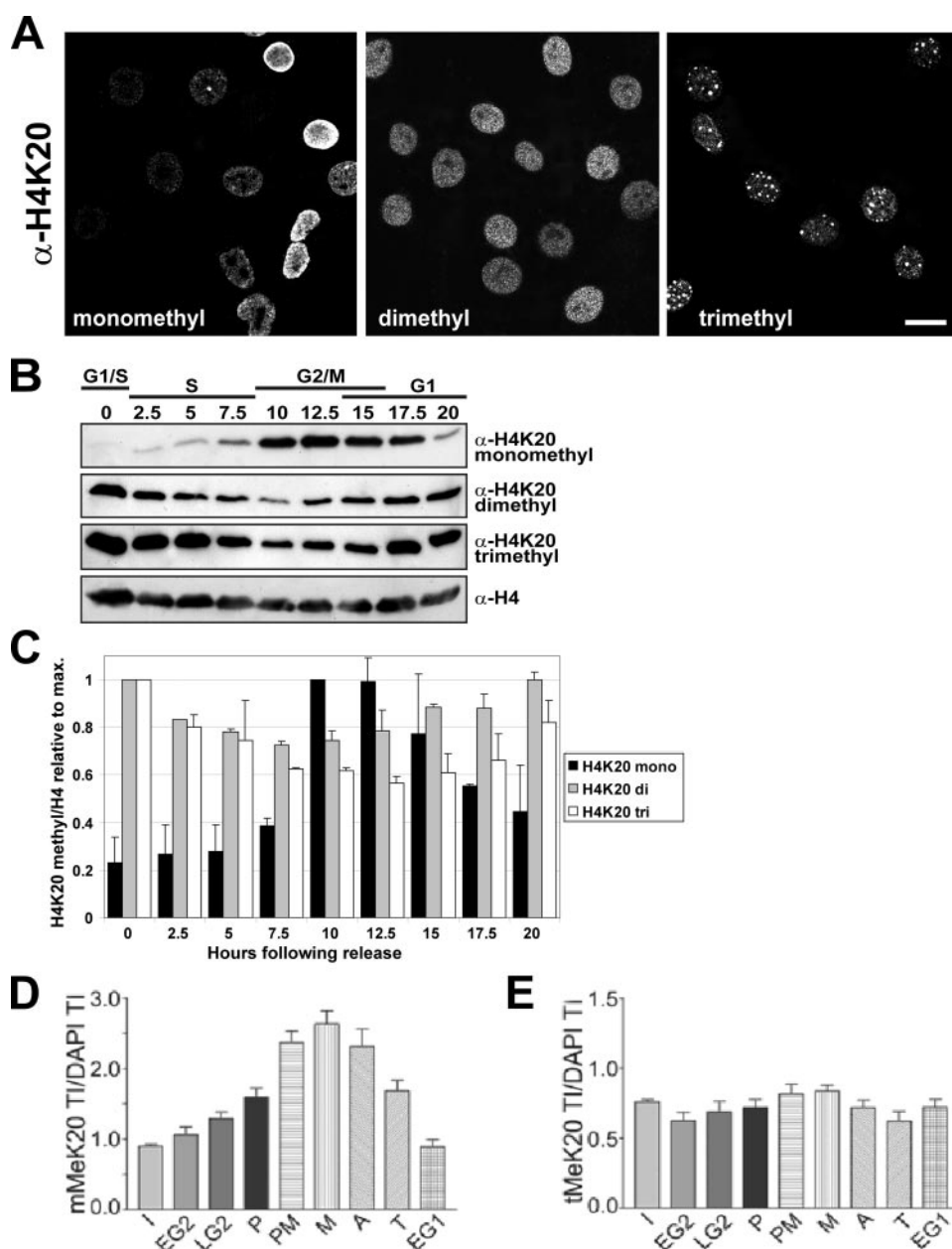


**FIGURE 1. Histone H4K20 monomethylation selectively occurs during G<sub>2</sub>/M.** *A*, nuclei of asynchronously dividing mouse embryonic fibroblasts were stained with either the mono-, di-, or trimethyl-specific H4K20 antibodies. The scale bar is 20  $\mu$ m. *B*, HeLa cells were arrested at the G<sub>1</sub>/S border by a thymidine-mimosine double block. Cells were collected every 2.5 h after release from block, and cell cycle status was determined by fluorescence-activated cell sorter. Whole cell lysates were fractionated by SDS-PAGE, and Western analysis was performed using the mono-, di-, and trimethyl-specific H4K20 antibodies; a general histone H4 antibody was used as a loading control. *C*, semi-quantitative analysis of the Western results. Integrated densitometry was used to determine the intensity of each H4K20 methyl band, which were then normalized relative to histone H4 for the corresponding time point. Biological replicates were performed to generate standard deviation. *D* and *E*, quantitative image microscopy was performed on 10T1/2 cells using the H4K20 monomethyl- or trimethyl-specific antibodies. DAPI-stained cells were first classified based on nine distinct cell cycle stages: interphase (I), early G<sub>2</sub> (EG<sub>2</sub>), late G<sub>2</sub> (LG<sub>2</sub>), prophase (P), prometaphase (PM), metaphase (M), anaphase (A), telophase (T), and early G<sub>1</sub> (EG<sub>1</sub>). The results are graphed as the mean methylation total signal intensity (TI)/mean DAPI total signal intensity (y axis) at each cell cycle stage (x axis)  $\pm$  standard error.

**MNase Digestion**—The cells were incubated in nuclear isolation buffer (150 mM NaCl, 10 mM HEPES, pH 7.5, 1.5 mM MgCl<sub>2</sub>, 10 mM KCl, 0.5% Nonidet P-40, 0.5 mM dithiothreitol) at 4 °C to release nuclei, which were resuspended in MNase digestion buffer (0.32 M sucrose, 50 mM Tris-HCl, pH 7.4, 4 mM MgCl<sub>2</sub>, 1 mM CaCl<sub>2</sub>) to a concentration of 0.5 mg/ml as deter-

mined by A<sub>260</sub>. Ten units of MNase/0.5 mg DNA was used for a 1-, 3-, or 5-min digestion prior to quenching with a final concentration of 10 mM EDTA. DNA was isolated before fractionation by agarose electrophoresis as previously described (37).

**GST Pulldown Assays**—The tandem tudor domains of 53BP1 (amino acids 1480–1616) were cloned into the pGEX4T-1 vector (Amersham Biosciences). GST fusion proteins were expressed in *Escherichia coli* by induction with 0.4 mM isopropyl  $\beta$ -D-thiogalactopyranoside (Sigma). The cells were sonicated on ice, and soluble lysate was used to batch purify GST fusion proteins using glutathione agarose (Sigma), followed by elution with 10 mM reduced glutathione in 50 mM Tris-HCl, pH 8.0. The purified GST or GST-53BP1-TT (5  $\mu$ g) was incubated with 200  $\mu$ g of purified HeLa nucleosomes for 1 h at 4 °C (37), incubated with glutathione agarose (Sigma), and washed extensively with phosphate-buffered saline. The bound material was eluted, fractionated by SDS-PAGE, and transferred to polyvinylidene difluoride membrane for Western analysis.

## RESULTS

**Global Changes in H4K20 Methylation Occur during Cell Cycle Progression**—In the first set of experiments, a panel of antibodies that selectively discriminate between the three methylated forms of H4K20 were used in indirect immunofluorescence studies in asynchronously dividing mouse embryonic fibroblasts (Fig. 1A). Consistent with our previous results, each of the methylated forms partitioned to distinct genomic regions (32). Although di- and trimethylated H4K20 showed little change in the intensity of staining across the cell cycle, the intensity of monomethylated H4K20 staining varied greatly between cells. The modification was easily observed in the condensed chromatin of mitotic figures but was significantly reduced in interphase cells. These observations strongly suggested that H4K20 monomethylation selectively increases as cells enter mitosis.

Cell synchronization studies were performed to further characterize the global changes in H4K20 monomethylation during cell cycle progression. HeLa cells were synchronized at the  $G_1/S$  border by a thymidine-mimosine double block (31). Cells were released from the block and collected every 2.5 h, and then flow cytometry was used to determine their phase in the cell cycle (supplemental Fig. S1). Western analysis was performed on the whole cell lysates from these cells using the H4K20 methyl-specific antibodies and a general H4 antibody to control for loading (Fig. 1B). Semi-quantitative analysis was performed by determining the signal intensity of each H4K20 methyl band relative to the signal intensity of the general H4 control at the corresponding time point. The results were plotted relative to the time point where the specific H4K20 methylated state was maximal: di- and trimethylation at 0 h and monomethylation at 10 h (Fig. 1C). Consistent with the immunofluorescence studies, we found that monomethylated H4K20 was comparatively low at the  $G_1/S$  border, increased during S phase, and dramatically increased to a maximum during  $G_2/M$ . As the cells returned to  $G_1$ , mono-methylated H4K20 declined. In contrast, the global levels of both di- and trimethylated H4K20 were highest at  $G_1/S$  and slowly declined as cells progressed through S phase, most likely because of the deposition of unmodified histones during DNA replication (38, 39). As cells cycled through mitosis, the levels of both steadily increased as they returned to  $G_1$ . These findings indicate that only the monomethylation of H4K20 is predominantly restricted to  $G_2/M$ .

To detail the precise timing of H4K20 monomethylation during cell cycle progression, quantitative imaging microscopy was performed in mouse 10T1/2 cells (35). Individual cells were first visually categorized into distinct cell cycle stages based on their DAPI staining, as previously described (40). Then the total signal intensity of methylated H4K20 in each cell was determined and normalized to the total signal intensity of DAPI staining in that cell. Consistent with our cell cycle analysis, we found that H4K20 monomethylation steadily increased during  $G_2$  through prophase then dramatically increased as cells entered pro-metaphase and remained high through anaphase (Fig. 1D). During the anaphase to telophase transition, there was a marked reduction in monomethylated H4K20 until it returned to basal levels at  $G_1$ . In contrast, H4K20 trimethylation levels remained relatively constant through the various stages of mitosis (Fig. 1E). Based on these findings, we conclude that H4K20 mono-methylation increases through  $G_2$ , peaks at mitosis, and rapidly declines following cell division.

*Cell Cycle Fluctuations in H4K20 Monomethylation Occur at Specific Loci*—Because we had demonstrated that global levels of monomethylated H4K20 fluctuate during the cell cycle, we also predicted that local changes in this histone modification would be altered during cell cycle progression. Using the same HeLa cells chemically arrested at  $G_1/S$  or synchronized to  $G_2/M$ , ChIPs were performed using either the monomethyl-specific H4K20 antibody, a histone H3 general antibody as the positive control, or rabbit IgG as the nonspecific negative control. Conventional PCR amplifications were performed on the enriched material at known H4K20 monomethyl positive and negative regions for two different human genes, PTTG1IP and BRD1 (Fig. 2, A and C). In every case, PCR amplification was

detected for the histone H3 positive control, whereas the IgG negative control failed to amplify (Fig. 2, B and D). As predicted, monomethylated H4K20 was detected at the positive peaks for both PTTG1IP and BRD1 at  $G_2/M$ . In contrast, PCR amplification of the negative regions of both genes was absent or severely reduced by comparison. Consistent with the global findings above, these data indicate that the methylated state of H4K20 significantly changes at these specific genomic loci during cell cycle progression. Because monomethylated H4K20 also functions in transcriptional regulation, it was predicted that genes enriched in this cell cycle-regulated modification would also alter their expression at distinct points in the cell cycle. However, expression analysis of HeLa cells arrested at  $G_1/S$  or  $G_2/M$  for eight known monomethylated H4K20 target genes revealed that there was no consistent or predictable correlation in the expression of these target genes to distinct points of the cell cycle (supplemental Fig. S4).

*The PR-Set7 H4K20 Monomethyltransferase Is Required for Cell Cycle Progression*—Because H4K20 monomethylation and the protein levels of the PR-Set7 H4K20 monomethyltransferase are tightly cell cycle regulated (supplemental Fig. S2), our findings predicted that both are required for proper cell division (31). To test this, HEK 293 cells were transfected with a puromycin-resistant control shRNA or an shRNA construct that specifically eliminates PR-Set7, resulting in a global loss of monomethylated H4K20 (Fig. 3A). Cell growth was monitored beginning 2 days following puromycin selection (Fig. 3B). Although the nontransfected cells and shRNA control cells displayed a normal growth curve, the growth rate of cells lacking PR-Set7 and monomethylated H4K20 declined over time consistent with a cell cycle arrest and death. Flow cytometry revealed striking changes in cells lacking PR-Set7 and monomethylated H4K20. These cell populations had a clear reduction in the proportion of  $G_1$  cells and a concomitant increase in the amount of S phase and  $G_2/M$  cells relative to control cells (Fig. 3C). Quantitative measurements of the flow cytometry data demonstrated that there was an ~18% decrease in the number of  $G_1$  cells and ~11 and ~12% increases in S phase and  $G_2/M$  cells, respectively, compared with control cells (Fig. 3D). Consistent with this, Western analysis demonstrated the activation of ATM in the PR-Set7 shRNA cells, which is known to occur during S phase and  $G_2/M$  arrests (Fig. 3E) (41). Therefore, our findings show that the lack of PR-Set7 and monomethylated H4K20 results in a cell cycle arrest or delay with cells amassing in S phase and  $G_2/M$ .

Based on these findings and the findings above demonstrating that H4K20 monomethylation peaks during mitosis, we predicted that the lack of PR-Set7 and monomethylated H4K20 would result in a mitotic arrest. Consistent with this, Western analysis revealed that the PR-Set7 shRNA cells had accumulated significant amounts of cyclin B compared with control cells, suggesting that they had not progressed through anaphase because cyclin B must be degraded by APC/C for this to occur (Fig. 3E) (42). Consistent with this, the levels of cdc2 and cdc2 phosphorylated on tyrosine 15 were unchanged in the PR-Set7 shRNA cells, suggesting the inability of the cells to progress to mitosis. To determine whether the defect in progression occurred at  $G_2$  or early mitosis, Western analysis was per-

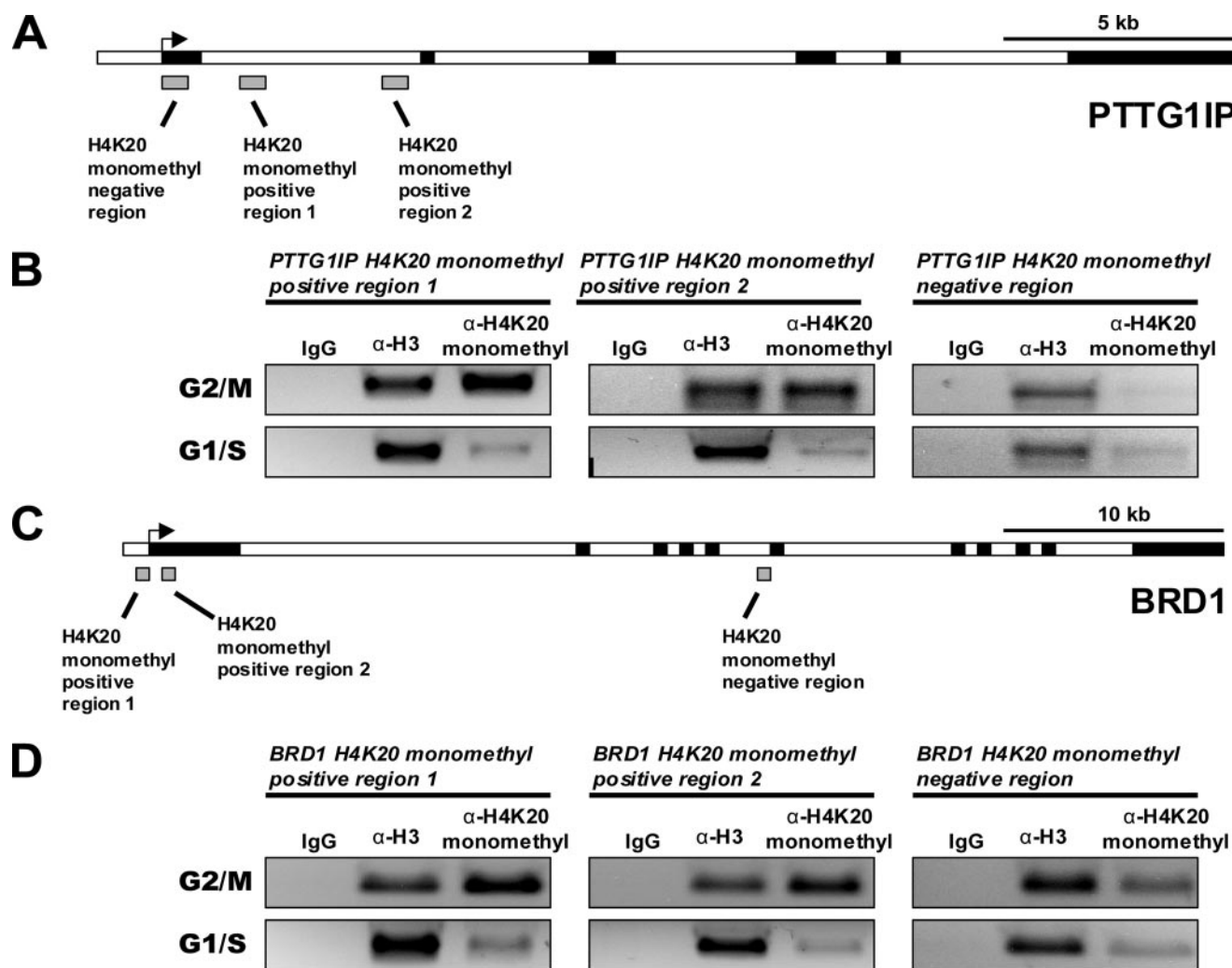


**FIGURE 2. Cell cycle-dependent changes in monomethylated H4K20 at specific loci.** Schematic representations of the human PTTG1IP gene (A) and BRD1 gene (C) are shown. The arrows indicate transcription start, and the black boxes represent exons. ChIPs were performed in synchronized HeLa cells (G<sub>1</sub>/S or G<sub>2</sub>/M) using either rabbit IgG, a histone H3 general antibody or the H4K20 monomethyl-specific antibody. PCR amplifications of the chromatin immunoprecipitated material were performed at the indicated H4K20 monomethyl positive and negative regions (gray boxes) for PTTG1IP (B) and BRD1 (D).

formed for phosphorylated histone H3 serine 28 (H3S28), a histone modification that specifically occurs at prophase during chromatin condensation and is reduced following metaphase (43). Our results demonstrate that the PR-Set7 shRNA cells displayed markedly decreased levels of phosphorylated H3S28 compared with control cells, indicating a failure to achieve the early stages of mitosis. Collectively, these findings show that the lack of PR-Set7 and monomethylated H4K20 results in an abnormal cell cycle profile where the cells are capable of completing DNA replication but are arrested or delayed at G<sub>2</sub> or the G<sub>2</sub>/M transition prior to prophase.

**Depletion of PR-Set7 Results in Decondensed Chromosomes and Centrosome Amplification**—To determine whether there were any aberrant morphological phenotypes associated with the loss of PR-Set7 and monomethylated H4K20, indirect immunofluorescence experiments were conducted. Visualization of nuclear DAPI staining revealed that the PR-Set7 shRNA cells stained less intensely and were much larger than control cells (Fig. 4A). Quantitative volumetric measurements indicate that the nuclei of the PR-Set7 shRNA cells were approximately

four times greater than control cells (Fig. 4B). Cells co-stained with the H4K20 monomethyl-specific antibody and  $\gamma$ -tubulin confirmed that cells with large nuclei lacked monomethylated H4K20 (Fig. 4C). Although the control cells displayed proper mitotic figures and high levels of monomethylated H4K20, the large nuclei of the PR-Set7 shRNA cells were nearly depleted of monomethylated H4K20 and contained decondensed chromosomes, consistent with a failure to achieve early mitosis. To confirm that the PR-Set7 shRNA cells failed to condense their chromosomes, nuclei from the different shRNA cells were treated with MNase, which efficiently digests DNA between nucleosomes when they are decondensed. Our findings demonstrate that the PR-Set7 shRNA cells are far more sensitive to MNase treatment as evidenced by the shift from oligonucleosomes to mononucleosomes compared with control shRNA cells, indicating a condensation failure (Fig. 4D). An unexpected yet striking phenotype of the PR-Set7 shRNA cells was the presence of multipolar spindles (Fig. 4C). Centrosome amplification can occur when cells are arrested in S or G<sub>2</sub> phases for prolonged periods, consistent with our findings (44,

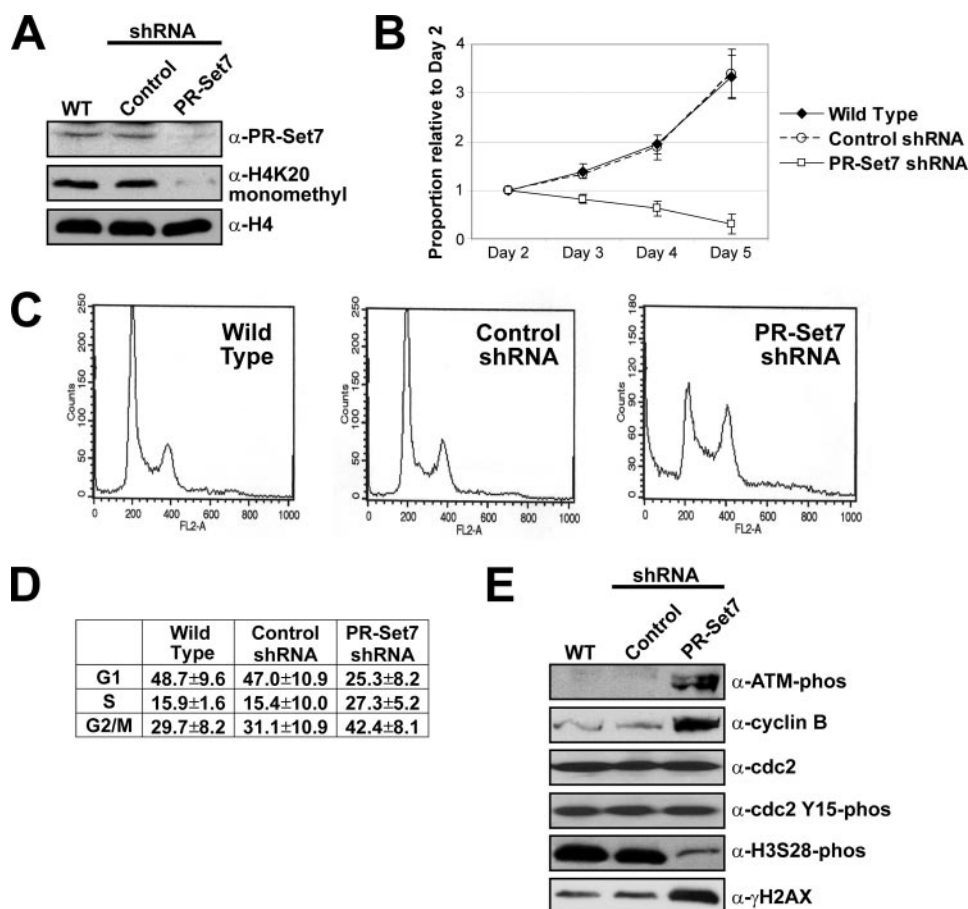


**FIGURE 3. PR-Set7 and monomethylated H4K20 are required for mitotic entry.** *A*, Western analysis of HEK 293 cells transfected with a puromycin-resistant control shRNA or a PR-Set7-specific shRNA construct that depletes cells of monomethylated H4K20. *B*, cell growth of shRNA transfected cells was measured 2 days after puromycin selection for 4 days (x axis) and plotted relative to the starting number of cells (y axis). *C*, transfected cells were stained with propidium iodide for flow cytometry analysis to visualize their cell cycle profile. *D*, three independent experiments were performed to calculate the average percentage of cells in each phase of the cell cycle. *E*, Western analysis of the transfected cells for phosphorylated ATM, cyclin B, cdc2, and cdc2 phosphorylated at tyrosine 15, phosphorylated H3S28, and  $\gamma$ H2AX.

45). Therefore, our findings strongly suggest that PR-Set7 monomethyltransferase activity plays a key role in chromosome condensation and that the loss of this activity results in genomic instability.

**Increased DNA Damage in the Absence of PR-Set7 and Monomethylated H4K20**—The observed increase in activated ATM suggested that the PR-Set7 shRNA cells were eliciting a DNA damage response. This was unexpected because it had been previously reported that DNA damage was not detected in *Drosophila* or *Schizosaccharomyces pombe* lacking the H4K20 methyltransferase ortholog (21, 46). Contrary to these findings, Western analysis demonstrated elevated levels of  $\gamma$ H2AX in the PR-Set7 shRNA cells compared with control cells clearly indicating DNA damage (Fig. 3E). Using the  $\gamma$ H2AX antibody in indirect immunofluorescence studies, we confirmed that the large nuclei of the PR-Set7 shRNA cells were selectively enriched in  $\gamma$ H2AX foci (Fig. 5A). In addition, single cell gel electrophoresis indicated an ~20-fold increase in the number of PR-Set7 shRNA cells containing DNA breaks compared with control cells (supplemental Fig. S3). Therefore, mammalian cells lacking PR-Set7 and monomethylated H4K20 undergo extensive DNA damage.

However, it remained unclear whether PR-Set7 actually played a direct role in the DNA damage response. We reasoned that if PR-Set7 was involved, then there should be an observable global increase in H4K20 monomethylation in normal cells exposed to DNA damaging agents. To test this, HEK 293 cells were exposed to various types of genotoxic stresses including ultraviolet light, hydrogen peroxide, camptothecin, and etoposide. In all cases, Western analysis demonstrated that DNA damage failed to alter global levels of monomethylated H4K20 (Fig. 5B and data not shown). These findings indicate that PR-Set7 and H4K20 monomethylation do not play a role in the global DNA repair response but rather suggest that they function to protect DNA and maintain genomic stability.

It was recently demonstrated *in vitro* that the conserved tandem tudor domains of the DNA repair protein, 53BP1, selectively bound mono- and dimethylated H4K20 peptides (20). To determine whether 53BP1 preferentially bound to mono- or dimethylated H4K20 in a more physiologically relevant context, a GST fusion protein containing the tandem tudor domains (TT) of 53BP1 was incubated with purified HeLa nucleosomes. Western analysis using a general H4 antibody on the GST-bound material indicated that GST-53BP1 TT efficiently bound nucleosomes compared with the GST-only negative control (Fig. 5C). Importantly, these nucleosomes were highly enriched in monomethylated H4K20 compared with dimethylated H4K20; trimethylated H4K20 was not detected. Therefore, these findings suggest that the observed increase in DNA damage in cells lacking PR-Set7 is due to the inability of 53BP1 to localize to damaged regions containing monomethylated H4K20. Consistent with this, the loss of PR-Set7 and monomethylated H4K20 resulted in the severe impairment of 53BP1 foci formation following DNA damage (20).

**Aberrant Phenotypes Associated with the Absence of PR-Set7 Occur Independently of p53**—It was recently reported that PR-Set7 can monomethylate p53 *in vivo* and negatively regulate its function (47). The report showed that the lack of PR-Set7 enhanced the proapoptotic and cell cycle checkpoint functions of p53. Therefore, it remained unclear whether the phenotypes we observed in the absence of PR-Set7 were due to the loss of H4K20 monomethylation or the loss of p53 methylation. To directly address this question, experiments were performed in

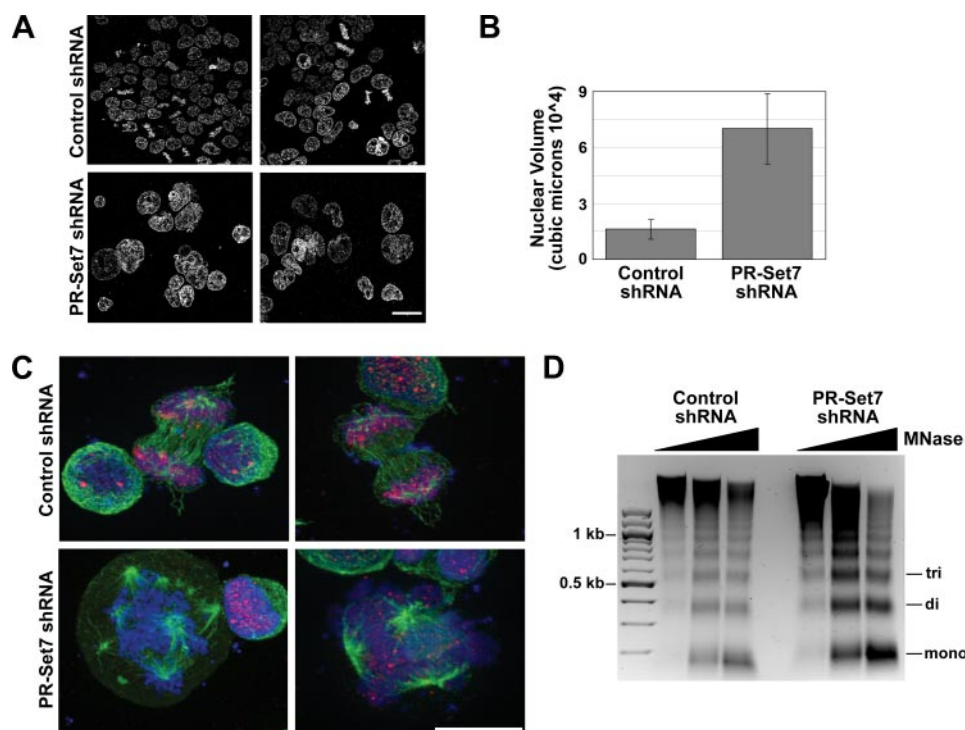


**FIGURE 4. Lack of PR-Set7 and monomethylated H4K20 results in decondensed chromatin and mitotic catastrophe.** A, DAPI staining of control shRNA HEK 293 cells or PR-Set7 shRNA cells containing abnormally large nuclei. The pictures were taken with a  $40\times$  objective at the same resolution. The scale bar is  $20\ \mu\text{m}$ . B, the total average nuclear volume was determined for the control and PR-Set7 shRNA HEK 293 cells. C, indirect immunofluorescence of the control and PR-Set7 shRNA HEK 293 cells was performed using the H4K20 monomethyl-specific antibody (red),  $\gamma$ -tubulin (green), and counterstained with DAPI (blue). The scale bar is  $20\ \mu\text{m}$ . D, nuclei from the control and PR-Set7 shRNA HEK 293 cells were digested with 10 units of MNase for 1, 3, or 5 min (triangle) prior to fractionation by agarose electrophoresis. The highest DNA fragments represent oligonucleosomes, and the lowest fragment corresponds to the size of a mononucleosome.

paired HCT116 cells that were either wild type p53 (WT) or where both copies of p53 were eliminated by homologous recombination (p53<sup>-/-</sup>) (48). Both cell types were transfected with either the control shRNA or the PR-Set7 shRNA that depletes cells of PR-Set7 and monomethylated H4K20 (Fig. 5D). Western analysis demonstrated an equal increase in the global levels of  $\gamma$ H2AX in both WT and p53<sup>-/-</sup> cells lacking PR-Set7. Similar to the HEK 293 cells, a dramatic decline in cell growth was observed in both WT and p53<sup>-/-</sup> cells lacking PR-Set7 compared with control cells (Fig. 5E). In addition, both cell lines also mimicked the other phenotypes of the HEK 293 cells in the absence of PR-Set7 including changes in the cell cycle profile, abnormally large nuclei deplete of monomethylated H4K20, chromosome decondensation, and centrosome amplification (data not shown). Collectively, these findings indicate that all of the observed aberrant phenotypes in cells lacking PR-Set7 are correlated with the loss of H4K20 monomethylation but are completely independent of p53 status.

**PR-Set7 Monomethyltransferase Activity Is Required for Cell Cycle Progression and Genomic Stability**—Because the shRNA experiments depleted cells of both PR-Set7 and monomethylated H4K20, it remained unclear whether the observed phenotypes were due to the lack of PR-Set7 enzymatic function. To determine this, HEK 293 cells were transfected with either a control vector expressing GFP or a vector expressing a catalytically dead (CD) PR-Set7 R265G point mutant that acts as a dominant negative by depleting monomethylated H4K20 with-

out reducing levels of PR-Set7 (Fig. 6A). Western analysis revealed significant elevated levels of  $\gamma$ H2AX in the PR-Set7 CD cells compared with GFP cells, indicating an increase in DNA damage, consistent with the PR-Set7 shRNA cells. In addition, flow cytometry demonstrated that the PR-Set7 CD cells had an  $\sim 12\%$  decrease in G<sub>1</sub> cells, an  $\sim 1\%$  increase in S phase cells, and an  $\sim 11\%$  increase in G<sub>2</sub>/M cells compared with the GFP control cells (Fig. 6B). The aberrant nuclear phenotypes observed in the PR-Set7 shRNA cells were also observed in the PR-Set7 CD cells: large nuclei lacking monomethylated H4K20, decondensed chromosomes, and centrosome amplification (Fig. 6C). Both the HCT116 WT and p53<sup>-/-</sup> cells transfected with the PR-Set7 CD construct displayed growth profiles similar to the PR-Set7 shRNA cells, demonstrating that the observed phenotypes are correlated to the lack of monomethylated H4K20 rather than p53 (Fig. 6D). Collectively, these findings demonstrate that the catalytic function of PR-Set7 is required for mitotic entry

and genomic stability independent of p53 status.

## DISCUSSION

Our findings demonstrate that PR-Set7-mediated monomethylation of histone H4K20 has a distinctive cell cycle profile that is required for proper cell cycle progression in mammalian cells. We found that PR-Set7 protein levels and monomethylated H4K20 are lowest in G<sub>1</sub> but rapidly rise during late S phase and peak precisely from prometaphase to anaphase. In contrast, di- and trimethylation of H4K20, most likely by the Suv4-20 enzymes (16), are highest at G<sub>1</sub> and decline during S and G<sub>2</sub>/M before returning to basal levels following cell division. Therefore, H4K20 monomethylation has a unique cell cycle profile compared with the other histone H4K20 methyl modifications.

One particularly interesting observation is the relatively rapid decrease in the levels of monomethylated H4K20 as cells exit mitosis and enter G<sub>1</sub>. In contrast to di- and trimethylated H4K20, this observation cannot be attributed to replication-associated deposition of unmodified histones because the cells are no longer in S phase. One possible explanation for the decrease in monomethylated H4K20 is the replication-independent exchange of modified histones with naïve histones (49). The observed “loss” of monomethylated H4K20 following mitosis would then be attributed to the absence of PR-Set7 during these phases of the cell cycle; it is not present to monomethylate naïve H4 (supplemental Fig. S2). However, this dilution theory may be unlikely because monomethylated H4K20 is typ-

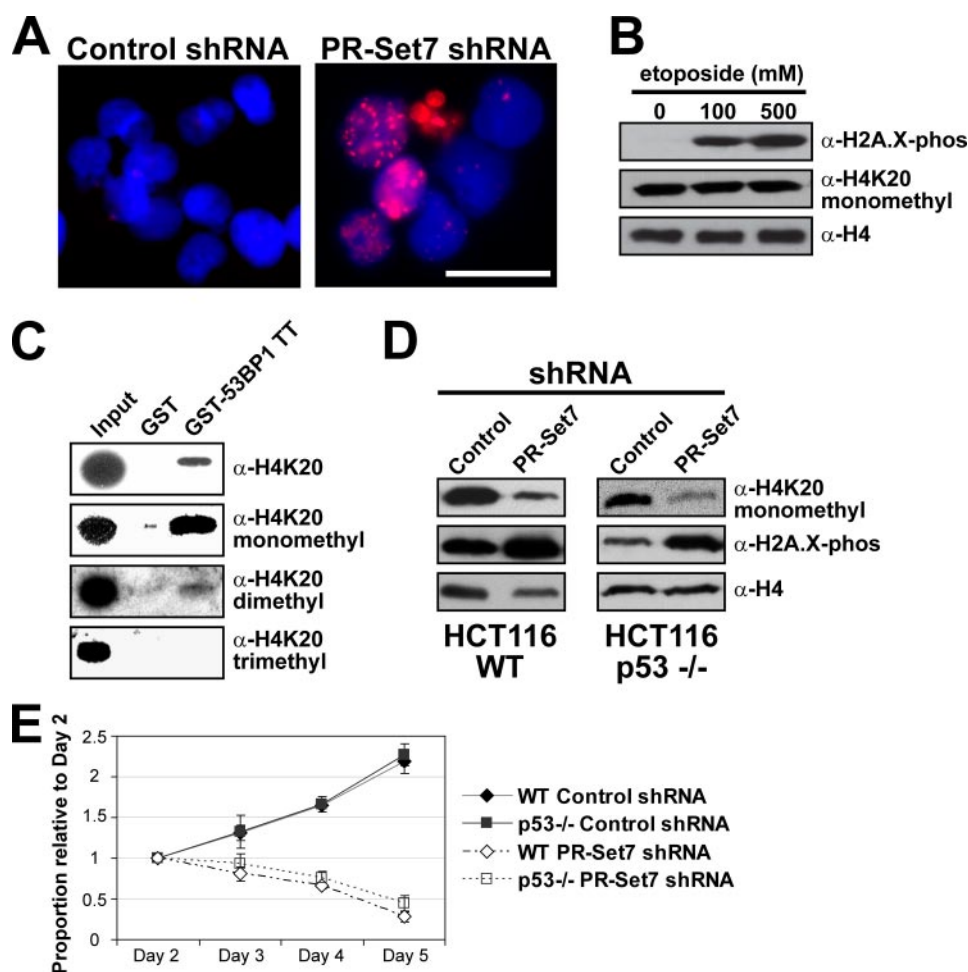


**FIGURE 5. Absence of PR-Set7 and monomethylated H4K20 results in DNA damage independent of p53 status.** *A*, indirect immunofluorescence of control shRNA or PR-Set7 shRNA HEK 293 cells for  $\gamma$ H2AX-associated damaged DNA (red) co-localized with nuclear DAPI staining (blue). The scale bar is 20  $\mu$ m. *B*, Western analysis of wild type HEK 293 cells for  $\gamma$ H2AX and monomethylated H4K20 following incubation with increasing amounts of etoposide for 2 h. *C*, purified HeLa nucleosomes were incubated with a GST fusion protein containing the tandem tudor domains of 53BP1 or GST alone as the control. Western analysis was performed on the GST-bound material. *D*, Western analysis of cell lysates from HCT116 wild type and p53 null cells transfected with either the control or PR-Set7 shRNA. *E*, growth curves of the transfected HCT116 cells measured 2 days after puromycin selection for 4 days (x axis) and plotted relative to the starting number of cells (y axis).

ically found in compacted chromatin, which is physically resistant to histone exchange. Another possible explanation is that an unknown H4K20 demethylase is active during this point in the cell cycle to rapidly decrease global levels of monomethylated H4K20. However, none of the currently identified histone demethylases impact H4K20, and all appear to act at a local level to regulate transcription rather than causing a global decrease in histone methylation (50). A third possibility is that monomethylated H4K20 serves as a preferred substrate for the di- and trimethylation of H4K20 by the Suv4-20 enzymes, as recently proposed (16, 51). This theory is consistent with our cell cycle findings where the apparent loss of monomethylated H4K20 is coincident with global increases in the di- and trimethylated forms as the cells exit mitosis. Although all three of these possibilities are not mutually exclusive, further investigations will need to be performed to determine which of them contributes to the loss of monomethylated H4K20 following mitosis.

whereas the mammalian form is a strict monomethyltransferase (22, 25).

Another difference between the response of flies and humans to the absence of PR-Set7 is DNA damage. It was previously shown that fly neuroblasts lacking PR-Set7 activated ATR; however, there was no indication of DNA damage in these cells (46). In contrast, we demonstrated that the absence of PR-Set7 and its enzymatic function in human cells results in the activation of ATM and an associated significant increase in damaged DNA. Because PR-Set7 was recently shown to also methylate p53 and regulate its function (47), it was highly likely that the observed cell cycle arrest and activation of DNA damage pathways in the absence of PR-Set7 was due to altered p53 function. However, in the paired wild type and p53<sup>-/-</sup> HCT116 cells lacking PR-Set7 enzymatic function, we observed the identical cell cycle defects and DNA damage regardless of p53 status, indicating that p53 methylation by PR-Set7 is not responsible for these phenotypes. Contrary to these findings, a recent

We also demonstrated that the loss of PR-Set7 H4K20 monomethyltransferase results in a G<sub>2</sub> arrest in mammalian cells, but surprisingly, *Drosophila* neuroblasts lacking PR-Set7 had a significant decrease in the number of cells in S phase and G<sub>2</sub>/M (46). The extremely low levels of cyclin B in these fly cells strongly suggested a G<sub>1</sub>/S arrest, whereas we observed in human cells lacking monomethylated H4K20 a substantial increase in cyclin B, indicative of a G<sub>2</sub>/M arrest. Interestingly, a proportion of the fly cells lacking PR-Set7 could escape this arrest/delay and proceed through mitosis; however, we were unable to identify any mitotic figures in human cells lacking monomethylated H4K20. Collectively, these findings suggest that humans have developed a significant role for PR-Set7 enzymatic function in the process of cell division compared with other eukaryotes. Consistent with this theory, *S. pombe* are viable in the absence of their PR-Set7 homolog and display marginal growth defects (21). One likely reason for these differences is the evolutionary specialization of the histone methyltransferases and their associated biological functions coincident with increased genome complexity. For example, the PR-Set7 homologs in *S. pombe* and *Api-complexan* are responsible for all three methylated forms of H4K20,

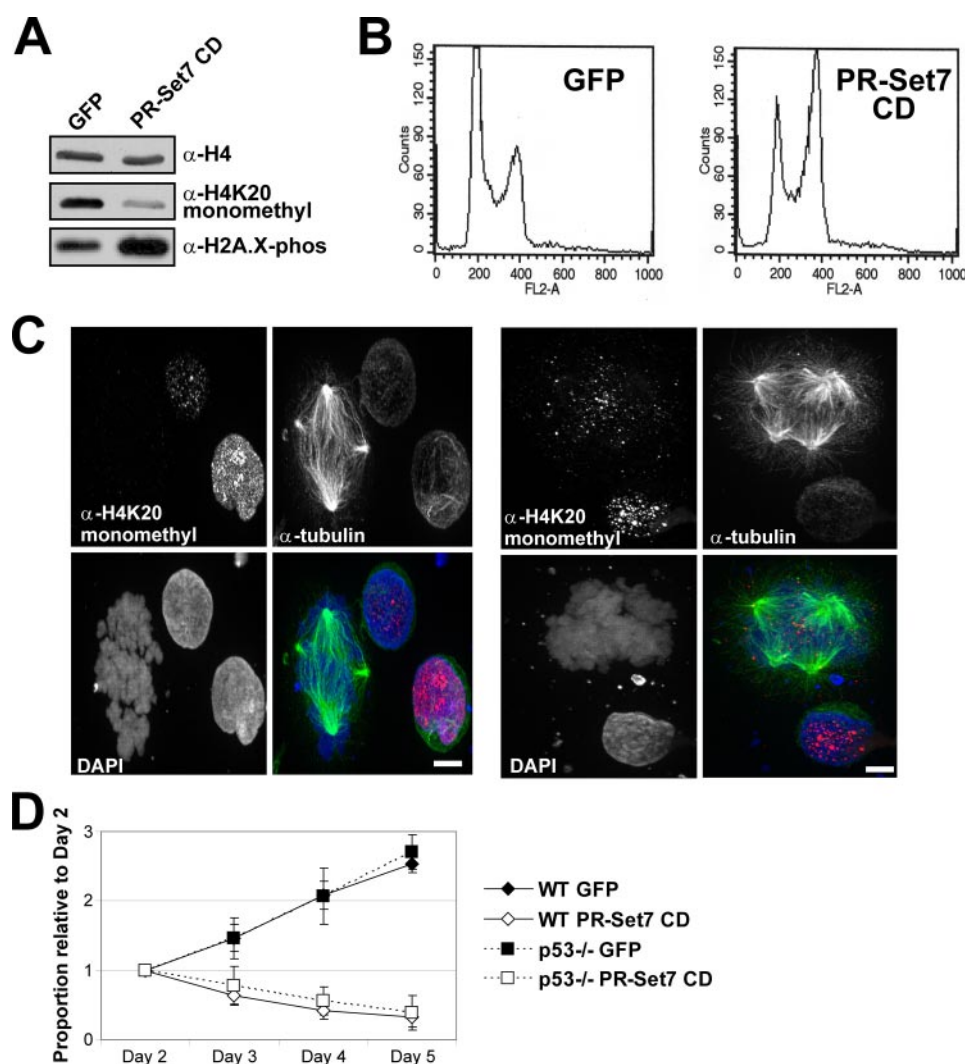


**FIGURE 6. H4K20 monomethylation is essential for cell cycle progression and genomic stability.** *A*, Western analysis for monomethylated H4K20 and  $\gamma$ H2AX on HEK 293 cells expressing GFP or a CD PR-Set7 R265G point mutant. *B*, the GFP and PR-Set7 CD transfected cells were stained with propidium iodide for flow cytometry analysis to visualize their cell cycle profile. *C*, indirect immunofluorescence of the PR-Set7 CD HEK 293 cells was performed using the H4K20 monomethyl-specific antibody (red),  $\gamma$ -tubulin (green), and counterstained with DAPI (blue). The scale bar is 20  $\mu$ m. *D*, growth curves of the HCT116 WT and p53 null cells transfected with GFP or PR-Set7 CD. Cell growth was determined 2 days after puromycin selection for 4 days (*x* axis) and plotted relative to the starting number of cells (*y* axis).

report demonstrated that inactivation of p53 by expressing the human papillomavirus oncoprotein E6 in human fibroblasts could partially suppress the G<sub>2</sub> arrest associated with the loss of PR-Set7 (30). Although the reasons for these differences remain unclear, the collective findings suggest that p53 is not sufficient to induce the observed G<sub>2</sub> arrest in cells lacking PR-Set7 and monomethylated H4K20.

Our findings strongly suggest that PR-Set7 monomethylation of H4K20 is a critical event for cell cycle progression and genomic stability. Although we speculated that PR-Set7-mediated H4K20 monomethylation played a role in the DNA repair process, we failed to detect changes in bulk levels of this histone modification following several types of genotoxic stresses. Our results indicate that they do not play a role in immediate DNA repair pathways but rather most likely serve a protective function. It has been proposed that this protective function is activated upon DNA damage where the breaks expose methylated

H4K20 to the nuclear environment (21). A recent report showed that the tandem Tudor domains of the 53BP1 repair protein specifically binds mono- and dimethylated H4K20 and that this interaction facilitates the repair process (20). In this report we demonstrate that 53BP1 preferentially binds nucleosomes enriched in monomethylated H4K20. Collectively, these results strongly suggest that the lack of monomethylated H4K20 does not necessarily cause DNA damage but makes cells more vulnerable to damage by preventing the proper localization of 53BP1 to sites of damage.

Our findings suggest that PR-Set7-mediated monomethylation of H4K20 plays a direct role in proper cell cycle progression and protection from DNA damage. However, possible indirect effects caused from the lack of PR-Set7 and monomethylated H4K20 cannot be discounted, especially because these also function to regulate the transcription of many unidentified genes (26). It is possible that the improper expression or repression of these genes in the absence of PR-Set7 may contribute to the observed phenotypes, but their direct roles in this process cannot be properly assessed until these genes are identified. Increasing reports demonstrate that histone-modifying enzymes can also modify proteins other than histones to regulate their functions (52). Therefore, it is plausible that PR-Set7 could methylate an unknown protein, other than histone H4, that functions in cell cycle progression and/or genomic stability. Although this is possible, previous findings clearly demonstrate that H4K20 is the major and preferential *in vivo* target of PR-Set7, strongly suggesting that H4K20 monomethylation is a critical event in proper cell cycle progression and protection from DNA damage (23, 24).

How could monomethylated H4K20 play a direct role in these biological processes? Increasing evidence indicates that histone modifications recruit and bind regulatory factors via conserved protein motifs and that this interaction is required for the observed biological effect (53). Indeed, we demonstrate in this report that the tandem tudor domains of 53BP1 preferentially bind monomethylated H4K20 nucleosomes, thereby predicting a model for protection from DNA damage. But what role does monomethylated H4K20 play in the cell cycle? Based on our findings and previous reports, we propose that this his-

tone modification plays a critical role in mitotic chromatin condensation. It was recently discovered that a human tumor suppressor protein called L3MBTL1 (lethal 3 malignant brain tumor-like 1) can specifically bind mono- and dimethylated H4K20 via a conserved malignant brain tumor motif (34, 54). Although it was shown that L3MBTL1 can associate with known chromatin condensation-related proteins *in vivo*, such as heterochromatin protein 1 and histone H1b, its direct interaction with methylated H4K20 was sufficient to cause chromatin condensation *in vitro*. Therefore, it is highly possible that the cell cycle-regulated H4K20 monomethylation by PR-Set7 serves to recruit and bind factors, such as L3MBTL1, that directly promote mitotic chromosome condensation. Following mitosis, PR-Set7 and monomethylated H4K20 levels dramatically decrease coincident with G<sub>1</sub>-associated chromatin decondensation. This paradigm is consistent with recent reports in the unicellular parasite, *Apicomplexa*, and *Drosophila* where the cell cycle profiles of H4K20 monomethylation are identical; the lack of PR-Set7 in flies results in abnormally high amounts of DNA and chromatin decondensation (33, 46, 55). Consistent with our findings, fly neuroblasts lacking PR-Set7 tended to accumulate in prophase and prometaphase and those that entered mitosis displayed lagging chromosomes, strongly suggesting that these cells were deficient for chromatin condensation. Therefore, the PR-Set7 monomethyltransferase activity appears to play a central role in cell cycle-dependent chromatin condensation, which is evolutionarily conserved among metazoans.

While this manuscript was under review, it was reported that PR-Set7 was targeted to replication foci by interacting with proliferating cell nuclear antigen and that PR-Set7 was required for proper DNA replication (28–30). However, our findings clearly demonstrate that PR-Set7 is only detectable and enzymatically active at G<sub>2</sub>/M. In addition, PR-Set7 appears to be selectively targeted for proteasome degradation during S phase (30). Therefore, these findings strongly suggest that PR-Set7 mainly functions in cell cycle progression during G<sub>2</sub>/M, when it is present and active. Although cells lacking PR-Set7 do display prolonged S phase progression, they are able to consistently complete DNA replication, but they are unable to proceed to mitosis, which again implies a central role for PR-Set7 at G<sub>2</sub>/M. Importantly, our findings indicate that the catalytic activity of PR-Set7 is essential for this process, most likely by monomethylating H4K20. This is supported by the observations that the cell cycle defects do not manifest until several cell cycles after depletion of PR-Set7 (29, 30). Our findings demonstrate that these defects are precisely correlated with the steady reduction of monomethylated H4K20 during these time points (supplemental Fig. S5). These findings predict that there is a specific threshold of monomethylated H4K20 that is required for mitotic chromatin condensation. This theory is consistent with a report from flies lacking PR-Set7 where they cease development at the third instar, the point at which the majority of the maternal stores of methylated H4K20 are exhausted (24).

Collectively, previous findings and our new observations strongly suggest a model where PR-Set7-mediated monomethylation of H4K20 is required for chromatin condensation for entry to prometaphase. Because condensed chromatin provides

inherent protection from intrinsic genotoxic stresses, the decondensed chromatin in the absence of monomethylated H4K20 would make DNA more susceptible to damage, as observed. It remains unclear whether the lack of PR-Set7 plays a direct role in centrosome amplification or if this occurs because of the prolonged G<sub>2</sub> arrest. Regardless, the aberrant centrosome amplification could result in chromosome segregation defects. This is consistent with findings that fly imaginal discs lacking PR-Set7 have a delayed cell cycle and the cells have a significant increase in DNA content, strongly suggesting aneuploidy (33). Therefore, mammalian cells with inappropriate doses of PR-Set7 and monomethylated H4K20 that escape the G<sub>2</sub> arrest and survive may result in daughter cells prone to a cancer phenotype. The failure to properly compact chromosomes could lead to gross chromosomal abnormalities, and the atypical increase in centrosomes could lead to aneuploidy during cell division, even in the presence of wild type p53. This possibility implies an important role for PR-Set7 and H4K20 monomethylation as tumor suppressors that function to prevent DNA damage and maintain genomic stability.

*Acknowledgments*—We thank Jonah Chan (University of Southern California) for assistance and use of the Zeiss Axio Imager Z1 microscope and analysis software. The PR-Set7 antibody was a gift from Danny Reinberg (New York University) and the H3S28-phos antibody was provided by Masaki Inagaki (Aichi Cancer Center). We thank Bert Vogelstein (Johns Hopkins) for the paired HCT116 WT and p53<sup>-/-</sup> cell lines.

## REFERENCES

1. Wolffe, A. P., and Guschin, D. (2000) *J. Struct. Biol.* **129**, 102–122
2. Murray, K. (1964) *Biochemistry* **3**, 10–15
3. Annunziato, A. T., Eason, M. B., and Perry, C. A. (1995) *Biochemistry* **34**, 2916–2924
4. Borun, T. W., Pearson, D., and Paik, W. K. (1972) *J. Biol. Chem.* **247**, 4288–4298
5. Camato, R., and Tanguay, R. M. (1982) *EMBO J.* **1**, 1529–1532
6. Hendzel, M. J., and Davie, J. R. (1989) *J. Biol. Chem.* **264**, 19208–19214
7. Hendzel, M. J., and Davie, J. R. (1991) *Biochem. J.* **273**, 753–758
8. Lee, N. M., and Loh, H. H. (1977) *J. Neurochem.* **29**, 547–550
9. Tidwell, T., Allfrey, V. G., and Mirsky, A. E. (1968) *J. Biol. Chem.* **243**, 707–715
10. Thomas, G., Lange, H. W., and Hempel, K. (1975) *Eur. J. Biochem.* **51**, 609–615
11. Ruthenburg, A. J., Allis, C. D., and Wysocka, J. (2007) *Mol. Cell* **25**, 15–30
12. Shinkai, Y. (2007) *Subcell. Biochem.* **41**, 337–350
13. Trievel, R. C. (2004) *Crit. Rev. Eukaryot. Gene Expr.* **14**, 147–169
14. Peters, A. H., Kubicek, S., Mechtler, K., O'Sullivan, R. J., Derijck, A. A., Perez-Burgos, L., Kohlmaier, A., Opravil, S., Tachibana, M., Shinkai, Y., Martens, J. H., and Jenuwein, T. (2003) *Mol. Cell* **12**, 1577–1589
15. Rice, J. C., Briggs, S. D., Ueberheide, B., Barber, C. M., Shabanowitz, J., Hunt, D. F., Shinkai, Y., and Allis, C. D. (2003) *Mol. Cell* **12**, 1591–1598
16. Schotta, G., Lachner, M., Sarma, K., Ebert, A., Sengupta, R., Reuter, G., Reinberg, D., and Jenuwein, T. (2004) *Genes Dev.* **18**, 1251–1262
17. Yang, H., Pesavento, J. J., Starnes, T. W., Cryderman, D. E., Wallrath, L. L., Kelleher, N. L., and Mizzen, C. A. (2008) *J. Biol. Chem.* **283**, 12085–12092
18. Delaval, K., Govin, J., Cerqueira, F., Rousseaux, S., Khochbin, S., and Feil, R. (2007) *EMBO J.* **26**, 720–729
19. Martens, J. H., O'Sullivan, R. J., Braunschweig, U., Opravil, S., Radolf, M., Steinlein, P., and Jenuwein, T. (2005) *EMBO J.* **24**, 800–812
20. Botuyan, M. V., Lee, J., Ward, I. M., Kim, J. E., Thompson, J. R., Chen, J.,

- and Mer, G. (2006) *Cell* **127**, 1361–1373
21. Sanders, S. L., Portoso, M., Mata, J., Bahler, J., Allshire, R. C., and Kouzarides, T. (2004) *Cell* **119**, 603–614
  22. Couture, J. F., Collazo, E., Brunzelle, J. S., and Trievel, R. C. (2005) *Genes Dev.* **19**, 1455–1465
  23. Fang, J., Feng, Q., Ketel, C. S., Wang, H., Cao, R., Xia, L., Erdjument-Bromage, H., Tempst, P., Simon, J. A., and Zhang, Y. (2002) *Curr. Biol.* **12**, 1086–1099
  24. Nishioka, K., Rice, J. C., Sarma, K., Erdjument-Bromage, H., Werner, J., Wang, Y., Chuikov, S., Valenzuela, P., Tempst, P., Steward, R., Lis, J. T., Allis, C. D., and Reinberg, D. (2002) *Mol. Cell* **9**, 1201–1213
  25. Xiao, B., Jing, C., Kelly, G., Walker, P. A., Muskett, F. W., Frenkiel, T. A., Martin, S. R., Sarma, K., Reinberg, D., Gamblin, S. J., and Wilson, J. R. (2005) *Genes Dev.* **19**, 1444–1454
  26. Barski, A., Cuddapah, S., Cui, K., Roh, T. Y., Schones, D. E., Wang, Z., Wei, G., Chepelev, I., and Zhao, K. (2007) *Cell* **129**, 823–837
  27. Vakoc, C. R., Sachdeva, M. M., Wang, H., and Blobel, G. A. (2006) *Mol. Cell. Biol.* **26**, 9185–9195
  28. Huen, M. S., Sy, S. M., van Deursen, J. M., and Chen, J. (2008) *J. Biol. Chem.* **283**, 11073–11077
  29. Jorgensen, S., Elvers, I., Trelle, M. B., Menzel, T., Eskildsen, M., Jensen, O. N., Helleday, T., Helin, K., and Sorensen, C. S. (2007) *J. Cell Biol.* **179**, 1337–1345
  30. Tardat, M., Murr, R., Herceg, Z., Sardet, C., and Julien, E. (2007) *J. Cell Biol.* **179**, 1413–1426
  31. Rice, J. C., Nishioka, K., Sarma, K., Steward, R., Reinberg, D., and Allis, C. D. (2002) *Genes Dev.* **16**, 2225–2230
  32. Sims, J. K., Houston, S. I., Magazinnik, T., and Rice, J. C. (2006) *J. Biol. Chem.* **281**, 12760–12766
  33. Karachentsev, D., Sarma, K., Reinberg, D., and Steward, R. (2005) *Genes Dev.* **19**, 431–435
  34. Trojer, P., Li, G., Sims, R. J., 3rd, Vaquero, A., Kalakonda, N., Boccuni, P., Lee, D., Erdjument-Bromage, H., Tempst, P., Nimer, S. D., Wang, Y. H., and Reinberg, D. (2007) *Cell* **129**, 915–928
  35. McManus, K. J., and Hendzel, M. J. (2005) *Methods* **36**, 351–361
  36. Nelson, J. D., Denisenko, O., Sova, P., and Bomsztyk, K. (2006) *Nucleic Acids Res.* **34**, e2
  37. Wu, S., Trievel, R. C., and Rice, J. C. (2007) *FEBS Lett.* **581**, 3289–3296
  38. Smith, P. A., Jackson, V., and Chalkley, R. (1984) *Biochemistry* **23**, 1576–1581
  39. Worcel, A., Han, S., and Wong, M. L. (1978) *Cell* **15**, 969–977
  40. McManus, K. J., Biron, V. L., Heit, R., Underhill, D. A., and Hendzel, M. J. (2006) *J. Biol. Chem.* **281**, 8888–8897
  41. Morgan, S. E., and Kastan, M. B. (1997) *Adv. Cancer Res.* **71**, 1–25
  42. Pines, J. (2006) *Trends Cell Biol.* **16**, 55–63
  43. Goto, H., Tomono, Y., Ajiro, K., Kosako, H., Fujita, M., Sakurai, M., Okawa, K., Iwamatsu, A., Okigaki, T., Takahashi, T., and Inagaki, M. (1999) *J. Biol. Chem.* **274**, 25543–25549
  44. Cheng, A., Balczon, R., Zuo, Z., Koons, J. S., Walsh, A. H., and Honkanen, R. E. (1998) *Cancer Res.* **58**, 3611–3619
  45. D'Assoro, A. B., Busby, R., Suino, K., Delva, E., Almodovar-Mercado, G. J., Johnson, H., Folk, C., Farrugia, D. J., Vasile, V., Stivala, F., and Salisbury, J. L. (2004) *Oncogene* **23**, 4068–4075
  46. Sakaguchi, A., and Steward, R. (2007) *J. Cell Biol.* **176**, 155–162
  47. Shi, X., Kachirskia, I., Yamaguchi, H., West, L. E., Wen, H., Wang, E. W., Dutta, S., Appella, E., and Gozani, O. (2007) *Mol. Cell* **27**, 636–646
  48. Bunz, F., Dutriaux, A., Lengauer, C., Waldman, T., Zhou, S., Brown, J. P., Sedivy, J. M., Kinzler, K. W., and Vogelstein, B. (1998) *Science* **282**, 1497–1501
  49. Linger, J., and Tyler, J. K. (2006) *Eukaryot. Cell* **5**, 1780–1787
  50. Klose, R. J., and Zhang, Y. (2007) *Nat. Rev. Mol. Cell Biol.* **8**, 307–318
  51. Pesavento, J. J., Yang, H., Kelleher, N. L., and Mizzen, C. A. (2008) *Mol. Cell. Biol.* **28**, 468–486
  52. Huang, J., and Berger, S. L. (2008) *Curr. Opin. Genet. Dev.* **18**, 152–158
  53. Jenuwein, T., and Allis, C. D. (2001) *Science* **293**, 1074–1080
  54. Kim, J., Daniel, J., Espejo, A., Lake, A., Krishna, M., Xia, L., Zhang, Y., and Bedford, M. T. (2006) *EMBO Rep.* **7**, 397–403
  55. Sautel, C. F., Cannella, D., Bastien, O., Kieffer, S., Aldebert, D., Garin, J., Tardieux, I., Belrhali, H., and Hakimi, M. A. (2007) *Mol. Cell. Biol.* **27**, 5711–5724